Broadband mode switch based on a three-dimensional waveguide Mach–Zehnder interferometer

HUANG, Quandong; JIN, Wei; CHIANG, Kin Seng

Published in:
Optics Letters

Published: 01/12/2017

Document Version:
Post-print, also known as Accepted Author Manuscript, Peer-reviewed or Author Final version

Published version (DOI):
10.1364/OL.42.004877

Publication details:
HUANG, Q., JIN, W., & CHIANG, K. S. (2017). Broadband mode switch based on a three-dimensional waveguide Mach–Zehnder interferometer. *Optics Letters*, *42*(23), 4877-4880. Advance online publication. https://doi.org/10.1364/OL.42.004877

Broadband mode switch based on three-dimensional waveguide Mach–Zehnder interferometer

QUANDONG HUANG, WEI JIN, AND KIN SENG CHIANG *

Department of Electronic Engineering, City University of Hong Kong, Hong Kong SAR, China
**Corresponding author: eeksc@cityu.edu.hk*

Received XX Month XXXX; revised XX Month, XXXX; accepted XX Month XXXX; posted XX Month XXXX (Doc. ID XXXXX); published XX Month XXXX

We propose a mode switch that operates on modulating the optical phases of a three-dimensional balanced four-arm waveguide Mach–Zehnder interferometer. We design and fabricate the device with polymer material to achieve thermo-optic switching between any two of the E_{11}, E_{21}, E_{12}, and E_{22} modes of the waveguide. Our experimental device shows an extinction ratio higher than 14 dB and a switching time shorter than 3.7 ms, measured with the E_{11} mode switched to any of the other modes at 1550 nm. This mode switch can operate over a wide range of wavelengths with weak polarization dependence and could be used in reconfigurable fiber-based mode-division-multiplexing systems, where mode routing is required.

OCIS codes: *(130.0130) Integrated optics; (130.4815) Optical switching devices; (130.5460) Polymer waveguides; (060.1810) Buffers, couplers, routers, switches.*

http://dx.doi.org/10.1364/OL.99.099999

Mode-division multiplexing (MDM), where different spatial modes of a few-mode fiber carry independent signals, is considered to be a promising technology to increase the transmission capacity of a single-mode fiber [1, 2]. The key device in an MDM system is a mode (de)multiplexer, which serves to combine or separate different modes at the input end or the output end of the system [3]. To fully exploit the capacity of MDM, the future MDM systems should be reconfigurable, where the mode channels are allowed to be switched temporally and/or spatially in response to the network traffic. In fact, an experimental reconfigurable MDM system based on the LP_{01}, LP_{11a}, and LP_{11b} modes has been demonstrated recently, where mode switching is achieved with a fixed mode multiplexer formed with a special three-core fiber directional coupler, followed by $LiNbO_3$ single-mode waveguide switches [4]. Mode switches that operate directly on two-mode waveguides based thermo-optic [5] and electro-optic [6–9] effects have also been reported. These devices, however, cannot be easily scaled to more spatial modes and, therefore, can only provide limited routing flexibility. There is a strong need to develop more effective mode switches, which can handle more spatial modes and provide more flexible switching functions. Recent studies based on different technologies [10–14] demonstrate that the spatial modes of a fiber or waveguide can be controlled particularly effectively with three-dimensional (3D) structures. In this letter, we propose a flexible 3D waveguide mode switching platform for the implementation of reconfigurable mode multiplexers.

Our proposed waveguide structure is a multi-arm Mach-Zehnder interferometer (MZI) formed with pairs of single-mode waveguides laid in different geometric layers. The single-mode waveguides are merged into few-mode waveguides at the two ends of the device with adiabatic waveguide branches. Thin-film electrode heaters are placed on the MZI arms to control the phases of the waves propagating along the arms by means of the thermo-optic effect. With this structure, any spatial mode launched into the MZI at one end can be converted into any other mode at the other end by controlling the electric currents applied to the respective electrodes. When this 3D MZI is integrated with a 3D waveguide multiplexer [12-14], spatial switching of the modes launched into the MZI can be achieved. The number of spatial modes that can be switched depends on the number of the arms and their layout in the 3D MZI. To demonstrate the principle and the features of the proposed structure, we design and fabricate a four-arm MZI with polymer material to achieve switching between any two of the E_{11}, E_{21}, E_{12}, and E_{22} modes (which correspond to the LP_{01}, LP_{11a}, LP_{11b}, and LP_{21a} modes of a fiber, respectively) in the C-band.

Figure 1(a) shows a schematic diagram of the proposed 3D mode switch, which is a symmetric, balanced four-arm MZI with two pairs of single-mode waveguide arms placed on two geometric layers. As shown in Fig. 1(a), Arm 1 and Arm 3 are placed on the upper level and Arm 2 and Arm 4 are placed on the lower level. The four arms have the same length and are merged into identical few-mode waveguides at both ends with cascaded horizontal (Y1) and vertical (Y2) symmetric Y-junctions at each end. In our design, the core and the cladding refractive indices are chosen to be n_{core} = 1.569 and $n_{cladding}$ = 1.559, respectively, which are the refractive indices of the polymer materials used for our experimental device. The width and the height of the few-mode core are 10 μm and 9 μm, respectively. The few-mode waveguide supports the E_{11}, E_{21}, E_{12}, and E_{22} modes, each of which can be polarized along the *x* direction (the TE polarization) or the *y* direction (the TM polarization). At the input end, the few-mode

core is divided into two halves by Y1 in the horizontal direction and each half is further divided into two halves by Y2 in the vertical direction. The cores of the four arms thus have a width of 5 μm and a height of 4.5 μm, which supports only the fundamental mode. The branching angles of Y1 and Y2 are 2.3° and 1.5°, respectively. S-bends are incorporated into the Y-junctions to provide sufficient separations among the four arms. At the output end, the four single-mode cores are combined into a few-mode core with another pair of Y2 and a Y1. The cross section of the device at the middle of the MZI together with the dimensions is shown in Fig. 1(b). Four thin-film electrode heaters, S1, S2, S3, and S4, are deposited on the surfaces of the four arms, respectively, to provide thermo-optic control of the refractive indices of the individual arms and hence the phases of the propagating waves.

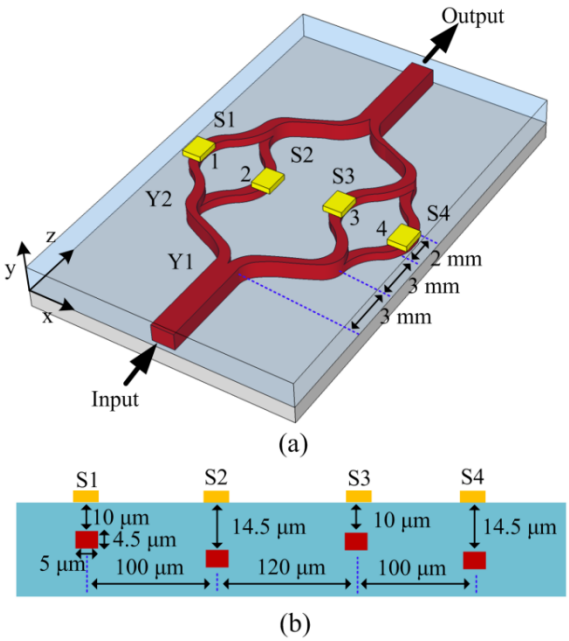

Fig. 1. Schematic diagrams showing (a) the structure of the proposed 3D MZI mode switch and (b) the cross section of the device at the middle of the MZI, together with the dimensions of the structure used in our design (not to scale).

When a guided mode of the few-mode core is launched into the device, its field is divided spatially into four equal parts by a set of Y-junctions, which propagate individually as the E_{11} modes in the respective arms of the MZI. They are combined at the output end by another set of Y-junctions and the combined field pattern depends on the phase differences introduced to the four arms by the electric currents applied to the electrode heaters. When there are no phase differences among the four arms, the output mode is the same as the input mode. When π-phase differences are introduced to certain arms, any of the four modes launched to the input end can be converted into any other mode at the output end. To facilitate discussion, we denote $\varphi1$, $\varphi2$, $\varphi3$, and $\varphi4$ as the phases in the four arms generated by the heaters S1, S2, S3 and S4, respectively. With $\varphi1 = \varphi2 = \varphi3 = \varphi4 = 0$ (S1, S2, S3, and S4 off), the output mode is the same as the input mode. With $\varphi1 = \varphi2 = \pi$ (S1 and S2 on) and $\varphi3 = \varphi4 = 0$ (S3 and S4 off), the E_{11} mode is converted into the E_{21} mode and vice versa, as this phase combination ensures that the left and the right half of the input field are out of phase by π at the output end. This same phase combination also allows the conversion between the E_{12} mode and the E_{22} mode. Similarly, the phase combination $\varphi1 = \varphi3 = \pi$ (S1 and S3 on) and $\varphi2 = \varphi4 = 0$ (S2 and S4 off), which ensures that the upper and the lower half of the input field are out of phase by π at the output end, allows the conversion between the E_{11} mode and the E_{12} mode or between the E_{21} mode and the E_{22} mode. Finally, the phase combination $\varphi1 = \varphi4 = \pi$ (S1 and S4 on) and $\varphi2 = \varphi3 = 0$ (S2 and S3 off) allows the conversion between the E_{11} mode and the E_{22} mode or between the E_{21} mode and the E_{12} mode. The switching functions of the device are summarized in Table 1. Although the present study focuses on the mode-switching functions of the device, the same device could be employed to convert between two arbitrary compositions of the four modes by properly controlling the phases of the waves in the four arms.

Table 1. Mode-Switching Functions of the Thermo-Optic 3D MZI for Different Phase Combinations.

Input	Output			
	$\varphi1=\varphi2=0$, $\varphi3=\varphi4=0$	$\varphi1=\varphi2=\pi$, $\varphi3=\varphi4=0$	$\Phi1=\varphi3=\pi$, $\varphi2=\varphi4=0$	$\varphi1=\varphi4=\pi$, $\varphi2=\varphi3=0$
E_{11}	E_{11}	E_{21}	E_{12}	E_{22}
E_{21}	E_{21}	E_{11}	E_{22}	E_{12}
E_{12}	E_{12}	E_{22}	E_{11}	E_{21}
E_{22}	E_{22}	E_{12}	E_{21}	E_{11}

We calculate the switching performance of the device with a 3D finite-difference beam propagation method (3DFD-BPM, RSoft). For the sake of simplicity, the loss and the dispersion of the material are ignored in our simulation. Assuming a thermo-optic coefficient of -8.0×10^{-5} /°C for the polymer material, a π -phase change at the wavelength 1550 nm in any arm of the MZI requires a temperature change of ~5 °C at the center of the core, which can be achieved by applying current to the electrode heater. Assuming that only the E_{11} mode is launched into the MZI, the transmission spectra of the device normalized to the E_{11} input power are shown in Fig. 2 for different switching states. As shown in Fig. 2(a), with all the switches turned off, the E_{11} mode suffers from a small radiation loss of 0.07 dB (or 1.5%), which is caused by the Y-junctions and the S-bends. With S1 and S2 turned on and S3 and S4 turned off, the E_{11} mode is converted into the E_{21} mode with a conversion efficiency of 99.84% and a mode extinction ratio higher than 28 dB over the C-band, as shown in Fig. 2(b). Similarly, with S1 and S3 turned on and S2 and S4 turned off, the E_{11} mode is converted into the E_{12} mode with a conversion efficiency of 99.80% and a mode extinction ratio higher than 27 dB, as shown in Fig. 2(c). Finally, with S1 and S4 turned on and S2 and S3 turned off, the E_{11} mode is converted into the E_{22} mode with a conversion efficiency of 99.75% and a mode extinction ratio higher than 26 dB, as shown in Fig. 3(d). The uniformity of the four output modes of the switch is within 0.49 dB over the C-band for the same E_{11} input power. The results are polarization-insensitive. The device performs similarly for other modes launched into the MZI. Although the device is optimized at 1550 nm (i.e., the phase change is exactly equal to π at 1550 nm), it shows excellent performance over the entire C-band and beyond, as shown in Fig. 2.

We fabricated the device with our in-house microfabrication facilities. We used the polymer materials EpoCore and EpoClad (Micro Resist Technology GmbH) as the core and the cladding material, respectively, whose refractive indices, measured with a

prism coupler (Metricon 2010) at 1536 nm, were 1.569 and 1.559, respectively (the refractive-index difference between the TE and TM polarizations was smaller than 0.001). The process of fabricating the 3D MZI is the same as that for the fabrication of the previously demonstrated 3D mode multiplexers [12-14] and, therefore, not elaborated here. With the 3D MZI made, chromium thin-film electrodes were formed on the four arms of the MZI by the process of plasma deposition (Desktop Pro, Denton Vacuum) and photolithography. Figure 3(a) shows an image of an end face of a fabricated device together with the core dimensions. As shown in Fig. 3(a), the upper and lower halves of the few-mode core are almost perfectly aligned. Figure 3(b) shows the thin-film electrodes deposited on the surface of the MZI that form the switches S1, S2, S3, and S4. The thickness, the width, and the length of each electrode are 120 nm, 20 μm, and 2000 μm, respectively. The total length of the fabricated device is about 25 mm.

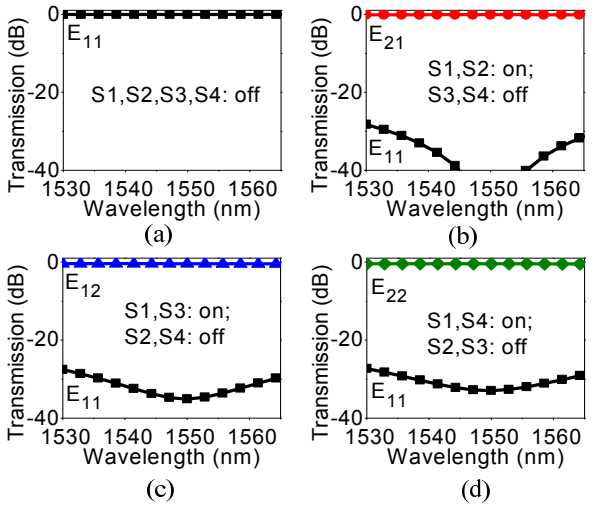

Fig. 2. Normalized transmission spectra of the thermo-optic 3D MZI calculated with the E_{11} mode as the input mode for different switching states: (a) S1, S2, S3, and S4 off; (b) S1 and S2 on, and S3 and S4 off; (c) S1 and S3 on, and S2 and S4 off; and (d) S1 and S4 on, and S2 and S3 off.

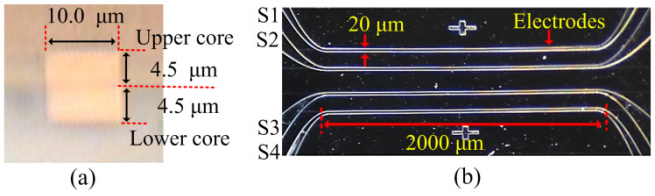

Fig. 3. Images of (a) an end face of a fabricated 3D MZI and (b) thin-film heater electrodes deposited on the four arms of the MZI for the realization of the switches S1, S2, S3, and S4.

To measure the performance of the fabricated device, light from a pigtailed tunable laser (KEYSIGHT) was launched into the device at one end to excite only the E_{11} mode of the few-mode core and the output from the other end was characterized. Figure 4 shows the output near-field patterns taken at three different wavelengths with an infrared camera, when S1, S2, S3, and S4 were tuned to achieve the best mode extinction ratios at 1550 nm. The electrical powers required for S1, S2, S3, and S4 to produce a π-phase change at 1550 nm were found to be 10.0, 10.5, 10.1, and 10.5 mw, respectively, which were insensitive to the polarization. The slightly larger switching powers of S2 and S4 were due to Arm 2 and Arm 4 locating in the lower level of the 3D structure. As shown in Fig. 4, the E_{11} mode can be switched to any of the other three modes by activating the required thermo-optic switches, which agrees with the expected switching functions of the device shown in Table 1. Because the mode conversion process is reversible, the results in Fig. 4 also confirm possible conversion from any of the high-order modes to the E_{11} mode.

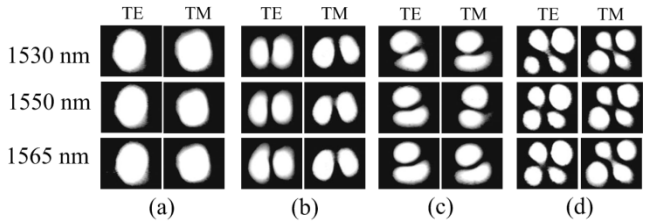

Fig. 4. Output near-field patterns taken at three wavelengths under different switching conditions for the TE and TM polarizations, when only the E_{11} mode was launched into the device: (a) S1, S2, S3, and S4 off; (b) S1 and S2 on, and S3 and S4 off; (c) S1 and S3 on, and S2 and S4 off; and (d) S1 and S4 on, and S2 and S3 off.

We next measured the transmission characteristics of the mode switch by monitoring the output light with a power meter through a short single-mode fiber (SMF), which had a core diameter of ~9 μm. We applied index-matching liquid at the fiber-waveguide interface to suppress Fresnel reflection and launched only the E_{11} mode into the device. By comparing the output powers measured with and without the SMF, the coupling loss between the SMF and the few-mode waveguide core was determined to be 0.5 dB at 1550 nm. The measured transmission spectra of the device normalized to the E_{11} input power for the TE polarization are shown in Fig. 5 for different switching states. With all the switches turned off, the E_{11} mode went through the device without converting into another mode and, as shown in Fig. 5(a), the E_{11} mode suffers from an insertion loss of 9.1 dB at 1550 nm, which is mainly the propagation loss. With S1 and S2 turned on and S3 and S4 turned off, as shown in Fig. 5(b), the E_{11} mode is converted into the E_{21} mode with a conversion efficiency of 97.4% and an insertion loss of 9.5 dB (which includes fiber-waveguide coupling losses at both ends) at 1550 nm, from which the mode extinction ratio is deduced to be 14.4 dB. Over the C-band, the mode extinction ratio is higher than 8.5 dB. Similarly, with S1 and S3 turned on and S2 and S4 turned off, as shown in Fig. 5(c), the E_{11} mode is converted into the E_{12} mode with a conversion efficiency of 97.2% and an insertion loss of 9.8 dB at 1550 nm. The mode extinction ratio is equal to 14.2 dB at 1550 nm and higher than 8.9 dB over the C-band. Finally, with S1 and S4 turned on and S2 and S3 turned off, as shown in Fig. 5(d), the E_{11} mode is converted into the E_{22} mode an efficiency of 98.8% and an insertion loss of 9.8 dB. The mode extinction ratio is equal to 16.5 dB at 1550 nm and higher than 14.3 dB over the C-band. To determine the "on" state of a switch, we tuned the electric current to the electrode of the switch till we obtained the minimum power output from the SMF at 1550 nm. We repeated the measurements for the TM

polarization and the efficiencies for the E_{11} mode to convert into the E_{21}, E_{12}, and E_{22} modes were 97.0%, 96.5%, and 99.1%, respectively, and the corresponding mode extinction ratios are 15.3, 13.5, and 17.3 dB, respectively, all measured at 1550 nm. The experimental results confirm that the device can operate over the C-band with low polarization dependence. While the results presented in Fig. 5 are optimized for operation at 1550 nm, the performance of the device at other wavelengths can be optimized by slightly tuning the switching powers. The fairly large insertion loss of the device is partly due to the polymer material used, which is developed mainly for application at 850 nm. It should be possible to significantly reduce the insertion loss of the device by improving the fabrication process and using low-loss polymer material developed for the C-band [15].

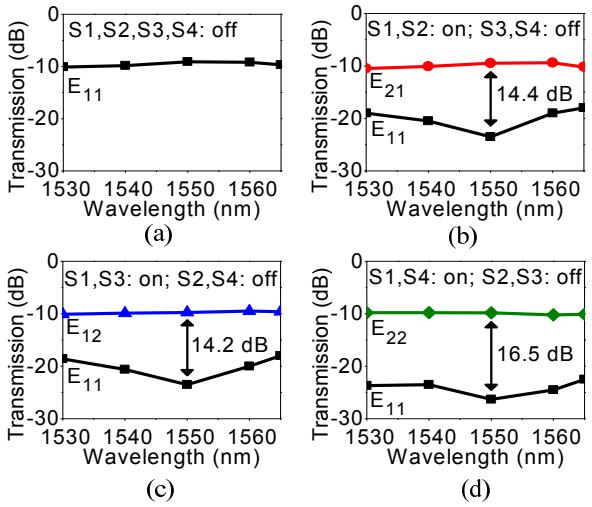

Fig. 5. Normalized transmission spectra of a fabricated thermo-optic 3D MZI measured with the E_{11} mode as the input mode for different switching states: (a) S1, S2, S3, and S4 off; (b) S1 and S2 on, and S3 and S4 off; (c) S1 and S3 on, and S2 and S4 off; and (d) S1 and S4 on, and S2 and S3 off.

We finally measured the switching speeds of the device by applying rectangular-wave electric currents to the switches and monitoring the output light with a power meter and an oscilloscope. As only two switches needed to be turned on for achieving the switching functions listed in Table 1, we used a single power supply to simultaneously drive the required two switches. Figure 6 shows the oscilloscopic displays of the output wave-forms for different switching states. As shown in Fig. 6, for the three switching functions considered, the rise time varies from 1.8 to 2.8 ms, while the fall time varies from 2.6 to 3.7 ms. Because the switching powers required for S1 and S3 are slightly lower than the other two, their switching times are also slightly shorter. The switching speed of our device is typical among the fast thermo-optic devices reported [16-18].

We have proposed a broadband thermo-optic mode switch based on the structure of a 3D multi-arm MZI. To demonstrate the salient features of the proposed structure, we have designed and fabricated a four-arm device with polymer material to achieve polarization-insensitive switching among the first four spatial modes of a few-mode waveguide. Our typical fabricated device offers mode-extinction ratios higher than 14 dB at 1550 nm and a switching time shorter than 3.7 ms. The switching power for each arm of the MZI is about 10 mW. The structure is scalable for more modes, as it allows a large few-mode core to be divided into more layers and each layer can accommodate many arms. When this 3D mode switch is integrated with a 3D mode (de)multiplexer [12–14], a switchable mode (de)multiplexer can be realized. Such functional devices should be useful for the development of reconfigurable MDM systems.

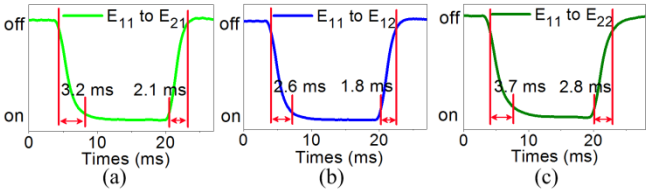

Fig. 6. Oscilloscopic displays of the temporal responses of the device for (a) E_{11}–E_{21} conversion (S1 and S2 on); (b) E_{11}–E_{12} conversion (S1 and S3 on); and (c) E_{11}–E_{22} conversion (S1 and S4 on).

Funding. Research Grants Council, University Grants Committee, Hong Kong (CityU 11253316).

References

1. D. J. Richardson, J. M. Fini, and L. E. Nelson, Nat. Photonics **7**, 354 (2013).
2. R. Essiambre, G. Kramer, P. J. Winzer, G. J. Foschini, and B. Goebel, J. Lightw. Technol. **28**, 662 (2010).
3. G. F. Li, N. Bai, N. B. Zhao, and C. Xia, Adv. in Opt. Photon. **6**, 413 (2014).
4. N. P. Diamantopoulos, M. Hayashi, Y. Yoshida, A. Maruta, R. Maruyama, N. Kuwaki, K. Takenaga, H. Uemura, S. Matsuo, and K. Kitayama, Opt. Express **23**, 23660 (2015).
5. W. Y. Chan and H. P. Chan, Opt. Express **22**, 9282 (2014).
6. W. Jin and K. S. Chiang, Opt. Lett. **40**, 237 (2015).
7. M. Zhang, K. Chen, W. Jin, and K. S. Chiang, Appl. Opt. **55**, 4418 (2016).
8. D. Melati, A. Alippi, and A. Melloni, Opt. Express **24**, 12625 (2016).
9. D. Melati, A. Alippi, A. Annoni, N. Peserico, and A. Melloni, Opt. Lett. **42**, 342 (2017).
10. N. Riesen, S. Gross, J. D. Love, and M. J. Withford, Opt. Express **22**, 29855 (2014).
11. A. M. Velazquez-Benitez, J. C. Alvarado, G. Lopez-Galmiche, J. E. Antonio-Lopez, J. Hernández-Cordero, J. Sanchez-Mondragon, P. Sillard, C. M. Okonkwo, and R. Amezcua-Correa, Opt. Lett. **40**, 1663 (2015).
12. J. Dong, K. S. Chiang, and W. Jin, J. Lightw. Technol. **33**, 4580 (2015).
13. J. Dong, K. S. Chiang, and W. Jin, Opt. Lett. **40**, 3125 (2015).
14. Y. Wu and K. S. Chiang, Opt. Lett. **42**, 407 (2017).
15. D. de Felipe, M. Kleinert, C. Zawadzki, A. Polatynski, G. Irmscher, W. Brinker, M. Moehrle, H. G. Bach, N. Keil, and M. Schell, J. Lightw. Technol. **35**, 683 (2017).
16. K. Chen, P. L. Chu, K. S. Chiang, and H. P. Chan, J. Lightw. Technol. **24**, 904 (2006).
17. X. Niu, Y. Zheng, Y. Gu, C. Chen, Z. Cai, Z. Shi, F. Wang, X. Sun, Z. Cui, and D. Zhang, Appl. Opt. **53**, 6698 (2014).
18. Z. Cai, B. Wang, Y. Zheng, M. Li, Y. Li, C. Chen, D. Zhang, Z. Cui, and Z. Shi, J. Mater. Chem. C **4**, 533 (2016).

References of the full version

1. D. J. Richardson, J. M. Fini, and L. E. Nelson, “Space-division multiplexing in optical fibres,” Nat. Photonics, 7, 354–362, (2013).
2. R. Essiambre, G. Kramer, P. J. Winzer, G. J. Foschini, and B. Goebel, “Capacity Limits of Optical Fiber Networks AND,” J. Lightw. Technol., 28(4), 662–701 (2010).
3. G. F. Li, N. Bai, N. B. Zhao, and C. Xia, “Space-division multiplexing: the next frontier in optical communication”, Advances in Optics and Photonics 6, 413-487 (2014).
4. N. P. Diamantopoulos, M. Hayashi, Y. Yoshida, A. Maruta, R. Maruyama, N. Kuwaki, K. Takenaga, H. Uemura, S. Matsuo, and K. Kitayama, "Mode-selective optical packet switching in mode-division multiplexing networks," Opt. Express **23**(18), 23660–23666 (2015).
5. W. Y. Chan and H. P. Chan, “Reconfigurable two-mode mux/demux device,” Opt. Express, **22**(8), 9282–9290 (2014).
6. W. Jin and K. S. Chiang, “Mode switch based on electro-optic long-period waveguide grating in lithium niobate,” Opt. Lett., **40**(2), 237-240 (2015).
7. M. Zhang, K. Chen, W. Jin, and K. S. Chiang, “Electro-optic mode switch based on lithium-niobate Mach-Zehnder interferometer,” Appl. Opt., vol. **55**(16), 4418-4422 (2016).
8. D. Melati, A. Alippi, and A. Melloni, “Reconfigurable photonic integrated mode (de)multiplexer for SDM fiber transmission,” Opt. Express, **24**(12), 12625–12634 (2016).
9. D. Melati, A. Alippi, A. Annoni, N. Peserico, and A. Melloni, "Integrated all-optical MIMO demultiplexer for mode- and wavelength-division-multiplexed transmission," Opt. Lett. **42**(2), 342–345 (2017).
10. N. Riesen, S. Gross, J. D. Love, and M. J. Withford, “Femtosecond direct-written integrated mode couplers,” Opt. Express **22**(24), 29855–29861 (2014)
11. A. M. Velazquez-Benitez, J. C. Alvarado, G. Lopez-Galmiche, J. E. Antonio-Lopez, J. Hernández-Cordero, J. Sanchez-Mondragon, P. Sillard, C. M. Okonkwo, and R. Amezcua-Correa, "Six mode selective fiber optic spatial multiplexer," Opt. Lett. **40**(8), 1663–1666 (2015).
12. J. Dong, K. S. Chiang, and W. Jin, “Compact Three-Dimensional Polymer Waveguide Mode Multiplexer,” J. Lightw. Technol., **33**(22), 4580–4588 (2015).
13. J. Dong, K. S. Chiang, and W. Jin, “Mode multiplexer based on integrated horizontal and vertical polymer waveguide couplers,” Opt. Lett. **40**(13), 3125–3128 (2015).
14. Y. Wu and K. S. Chiang, “Ultra-broadband mode multiplexers based on three-dimensional asymmetric waveguide branches,” Opt. Lett., **42**(3), 407–410 (2017).
15. D. de Felipe, M. Kleinert, C. Zawadzki, A. Polatynski, G. Irmscher, W. Brinker, M. Moehrle, H. G. Bach, N. Keil, and M. Schell, "Recent Developments in Polymer-Based Photonic Components for Disruptive Capacity Upgrade in Data Centers," J. Lightw. Technol. **35**(4), 683–689 (2017).
16. K. Chen, P. L. Chu, K. S. Chiang, and H. P. Chan, "Design and Fabrication of a Broadband Polymer Vertically Coupled Optical Switch," J. Lightw. Technol. **24**(2), 904-911 (2006).
17. X. Niu, Y. Zheng, Y. Gu, C. Chen, Z. Cai, Z. Shi, F. Wang, X. Sun, Z. Cui, and D. Zhang, "Thermo-optic waveguide gate switch arrays based on direct UV-written highly fluorinated low-loss photopolymer," Appl. Opt. **53**(29), 6698–6705 (2014).
18. Z. Cai, B. Wang, Y. Zheng, M. Li, Y. Li, C. Chen, D. Zhang, Z. Cui, and Z. Shi, "Novel fluorinated polycarbonate negative-type photoresists for thermo-optic waveguide gate switch arrays," J. Mater. Chem. C **4**(3), 533–540 (2016).